

Adaptive radial basis function generated finite-difference on non-uniform nodes using p -refinement

Leevan Ling^a and Pankaj K. Mishra^b and Siqing Li^c and Xin Liu^d and Jing Zhang^c and Mrinal K. Sen^d

^aDepartment of Mathematics, Hong Kong Baptist University, Hong Kong.

^bGeological Survey of Finland.

^cCollege of mathematics, Taiyuan University of Technology.

^dThe University of Texas at Austin, USA.

ARTICLE HISTORY

Compiled May 16, 2023

ABSTRACT

Radial basis function generated finite-difference (RBF-FD) methods have been gained popularity recently. For the approximation order of RBF-FDs' weights on scattered nodes, one can find mathematical theories in the literature. Many practical problems in numerical analysis, however, do not have a uniform node-distribution. Instead, it would be better suited if a relatively higher node-density is imposed on specific areas of domain where complicated physics needed to be resolved. In this paper, we propose a practical adaptive RBF-FD with a user defined convergence order with respect to the total number data points N . Our algorithm can output a sparse differentiation matrix system with the desired approximation order. Numerical examples about elliptic and parabolic equations are provided to show that the proposed adaptive RBF-FD method yields the expected convergence order. The proposed method reduces the number of non-zero elements in the linear system without sacrificing the accuracy. Furthermore, we apply our adaptive RBFFD method to the elastic wave models and obtain the desired convergence order.

KEYWORDS

Partial differential equations, radial basis functions, adaptive RBF-FD, scattered data, nodes reduction, convergence

MSC codes: 35J05, 35K20, 65N35.

1. Introduction

Radial basis functions (RBFs) have been a vital choice in the development of kernel-based meshless methods for solving partial differential equations (PDEs) numerically. The RBF-FD method is one such local meshless method, which has been gained popularity recently. Numerical evidences collected in recent years by a rapidly growing community of researchers suggest that the RBF-FD method offers numerical stability

L.L. Email: lling@hkbu.edu.hk

P.K.M. Email: pankajkmishra01@gmail.com

S.L. Email: lisiqing@tyut.edu.cn

X.L. Email: lx2wqy@utexas.edu

on irregular node layouts, high computational speed, high accuracy, easy local adaptive refinement, and excellent opportunities for large-scale parallel computing.

The basic idea of RBF-based differentiation can be traced back to [27] and formally as the RBF-FD to [28]. Since then, a significant amount of research has been dedicated towards the robust development of the RBF-FD [2, 3, 8, 10, 11, 18, 20, 21, 24, 29] and its application to solve various problems in science and engineering [4, 7, 9, 12–16, 25, 26]. Besides RBF-FD method, other collocation methods based on radial basis functions are also proposed to solve the PDEs. For example, a global radial basis function collocation method in [5] was successfully applied to solve computational fluid dynamic problem, and the local RBF collocation methods were used to solve the diffusion problem in [6] and the Hamiltonian PDEs in [31].

A major advantage of the RBF-FD method is that it works with scattered nodes, where each stencil can have a different configuration. This overcomes the fixed grid/element limitation of conventional numerical methods for solving PDEs. Unlike global meshless methods, the weights in the RBF-FD are computed locally using RBFs, which are expanded at some fixed number of nearest nodes. Once the weights at each node are computed, they can be stored and used for next-step computation, which makes weight computation a pre-processing step in solving time dependent PDEs by RBF-FD. Moreover, computations of weights at each node are independent processes, which makes RBF-FD to be the desired method for parallel computing.

In recent studies [2, 8], it has been demonstrated that combining high-order polynomials with polyharmonic spline radial basis functions (PHS+Poly) in the RBF-FD formulation led to considerable improvements in robustness. Some key benefits of the PHS+Poly approach are as follows:

- 1 It is free shape parameter, which simplifies the formulation and eliminates the need for fine-tuning;
- 2 It is efficiency compared to stable RBF-FD formulation based on infinitely smooth RBFs [21],
- 3 This method ensures accuracy near boundaries without the need for ghost-nodes where the stencils can become highly one-sided [1];
- 4 It has the potential of maintaining the accuracy for large and sparse linear systems;
- 5 The convergence order of the method depends mainly on the degree of the augmented polynomial, which also determines the size of the stencil.

In a structured node-layout, the order of the convergence has been numerically established. However, the convergence of the RBF-FD on non-uniform nodes needs some careful considerations. In the paper, we propose an adaptive RBF-FD algorithm, which is customized to a user-defined global convergence order with respect to the number of nodes in the domain. In particular, we provide an method to obtain the user-defined convergence order in a highly non-uniform node-layout with significantly large mesh ratio¹. Besides the above listed benefits, we will use the PHS+Poly approach adaptively in the present work so that we can control the order of convergence with a single variable, viz., the degree of augmented polynomial. From here and on, by the term RBF-FD, we mean the RBF-FD formulated using PHS + Poly approach. To generate such non-uniform and adaptive nodes, we use a downloadable package — **NodeLab** [17] by the presented author.

The rest of the paper is organized as follows. We discuss the general formulation of the

¹The ratio of fill-distance over minimum separating distance, whose role is similar to the mesh-ratio in the context of finite element methods

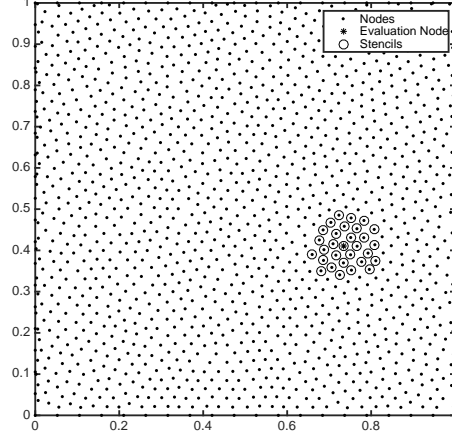


Figure 1.: A prototype figure showing centres and local stencil.

RBF-FD, polynomial augmentation and some insights for its stable implementation in Section 2. In Section 3, we give a precise definition of the global order of the convergence in an non-uniform node-layout. We also provide a method that connects the global convergence order to the required degree of polynomial at a local scale depending on the local fill distance. This is followed by a discussion of the weight computation approach through the adaptive RBF-FD method. In Section 4, we provide numerical examples to support the advantages of the proposed method, and followed by conclusions in Section 5.

2. RBF-FD approximation

As a review, in the following, we discuss the standard RBF-FD

Consider a computational domain Ω , within which we have distinctly scattered nodes $X := \{\mathbf{x}_1, \mathbf{x}_2, \dots, \mathbf{x}_N\} \in \mathbb{R}^d$. For linear differential operator \mathcal{L} and $1 \leq c \leq N$, in order to approximate the values of $\mathcal{L}u$ at center point $\mathbf{x}_c \in X$, we need to compute RBF-FD weights $\mathbf{w}_c := \{w_1^c, w_2^c, \dots, w_N^c\}$ at center point \mathbf{x}_c using function values of u at some subset of X , that is commonly referred to as the stencil of \mathbf{x}_c consisting neighbour nodes of \mathbf{x}_c and itself. The number of nonzero elements in \mathbf{w}_c is the stencil-size of \mathbf{x}_c , denoted by n_s^c . We denote the stencil of \mathbf{x}_c by $X_c := \{\mathbf{x}_1^c, \dots, \mathbf{x}_{n_s^c}^c\} \subseteq X$ and we can write the $\mathcal{L}u(\mathbf{x}_c)$ as

$$\mathcal{L}u(\mathbf{x}_c) \approx \sum_{k=1}^{n_s^c} w_k^c u(\mathbf{x}_k^c) = \mathbf{w}_c u|_{X_c}. \quad (1)$$

Figure 1 shows the prototype of the scatter data distribution and local stencil of the evaluation node. At this stage, the task is to compute the weight \mathbf{w}_c that gives a good approximation in the sense of (1). With some radial basis function $\phi : [0, \infty) \rightarrow \mathbb{R}$, the standard RBF-FD approach computes these weights by solving the following linear

system

$$\underbrace{[\phi(\|\mathbf{x}_i^c - \mathbf{x}_j^c\|)]_{1 \leq i, j \leq n_s^c}}_{=: A_c} \mathbf{w}_c^T = \underbrace{[L\phi(\|\mathbf{x} - \mathbf{x}_i^c\|)|_{\mathbf{x}=\mathbf{x}_c}]_{1 \leq i \leq n_s^c}}_{=: L\phi|_{\mathbf{x}_c}}. \quad (2)$$

If ϕ is symmetric positive definite (SPD), ~~then~~ the interpolation matrix A_c ~~must~~ also be SPD and hence (2) is uniquely solvable. It is shown in [22] that (2) is error optimal in the native space norm corresponding to the radial basis function ϕ . We refer readers to the article for details.

2.1. The RBF-FD (PHS+Poly) approach

Unlike global meshless methods, the local nature of the RBF-FD rules out the exponential² convergence even with infinitely smooth RBFs. With the motivations discussed in [23] and earlier in this paper, using a conditionally positive definite kernel with finite order of smoothness, like PHS ($\phi(r) = r^{2m+1}$; $m = 1, 2, 3, \dots$), is reasonable in the RBF-FD method. We also augment polynomial basis of sufficient degrees in order to ensure exact reproduction of low order polynomials. To compute RBF-FD weights in Eq. (1) by PHS and polynomials, we enforce the Eq. (1) to be exact for the following interpolation $I(\mathbf{x})$

$$I(\mathbf{x}) \approx \sum_{k=1}^{n_s^c} \lambda_k \phi(\|\mathbf{x} - \mathbf{x}_k\|) + \sum_{l=1}^{n_p^c} \gamma_l p_l(\mathbf{x}), \quad (3)$$

subject to the constraints

$$\sum_{k=1}^{n_s^c} \gamma_l p_l(\mathbf{x}_k) = 0, \quad l = 1, 2, 3, \dots, n_p^c, \quad (4)$$

where n_s^c is the stencil-size of \mathbf{x}_c and n_p^c is number of augmented multivariate polynomial basis, see Table 1 for 2D case and [8] for 1D and 3D cases. The augmented version of the linear system (2) is given as

$$\begin{bmatrix} A_c & P_c \\ P_c^T & O \end{bmatrix} \begin{bmatrix} \mathbf{w} \\ \mathbf{w}_e \end{bmatrix} = \begin{bmatrix} L\phi|_{\mathbf{x}_c} \\ L\mathbf{p}|_{\mathbf{x}_c} \end{bmatrix}, \quad (5)$$

where A_c and $L\phi|_{\mathbf{x}_c}$ are as in (2). The $n_s^c \times n_p^c$ matrix P_c and $n_p^c \times 1$ vector $L\mathbf{p}|_{\mathbf{x}_c}$ are given as

$$P_c = [p_j(\mathbf{x}_i^c)]_{1 \leq i \leq n_s^c, 1 \leq j \leq n_p^c}, \quad \text{and} \quad L\mathbf{p}|_{\mathbf{x}_c} = [Lp_l(\mathbf{x})|_{\mathbf{x}=\mathbf{x}_c}]_{1 \leq l \leq n_p^c}.$$

From here and on, we drop the super/subscript “c” from our notations for simplicity and all computations need to go center by center for all $\mathbf{x}_c \in X$. The number of polynomial basis (n_p) for the space of d -dimensional polynomials up to degree p is

²for the approximation of a function lying in a certain native space

Table 1.: Understanding the number of polynomial terms based the degree of polynomial to be augmented.

Polynomial degree (p)	Polynomial basis	$n_p = C(p + 2, 2) = \frac{(p+2)!}{p!2!}$
0	1	1
1	$1, x, y$	3
2	$1, x, y, x^2, y^2, xy$	6
3	$1, x, y, x^2, y^2, xy, x^3, y^3, x^2y, xy^2$	10
4	\dots	15
5	\dots	21
\vdots	\vdots	\vdots

given by

$$n_p = C(p + d, d) = \frac{(p + d)!}{p!d!}. \quad (6)$$

Table 1 lists out the number of polynomial terms for different degrees of polynomials, for a two-dimensional case ($d = 2$). For example, $n_p = 3$ in 2D, corresponds to appending polynomial up to first order. Equation (5) can be interpreted as an equality-constrained quadratic programming problem (see [2] for more details on this).

2.2. Stencil-size and Stagnation error

It has been found in [2, 8] that, the convergence order of RBF-FD was governed by the degree of augmented polynomial p ; while the order of the PHS RBF has a marginal effect on the accuracy and no influence to the order of convergence. Moreover, when the order of augmented polynomial is fixed and sufficient high, increasing n_s – beyond what is required³, does not improve the accuracy or the convergence order, significantly. In case the augmented polynomial is of lower-order, increasing n_s could lead to marginal improvement in the accuracy; however, the convergence order practically remains unaffected. Such an specific independence on the stencil size becomes vital for the adaptivity. That is, in sub-domains with higher node-density, we could use a smaller degree of augmented polynomial (and therefore smaller n_s) – locally, without any significant loss in the convergence.

The above criterion for choosing the stencil-size, however, is recommended for node-distributions having ghost-nodes outside the boundary. The recommended rule of thumb for ensuring the stability of RBF-FD, without any special boundary treatment is $n_s \geq 2n_p$ [2, 8] to:

1. get the expected order of accuracy everywhere in the domain including the evaluation points near boundaries, where stencils are highly one-sided with respect to the evaluation point;
2. maintain the numerical stability to sparse linear systems for large-scale problems.

The stagnation error can be disrupted in the convergence under node-refinement, which

³to support the bases of the augmented polynomial (i.e. $n_s = n_p$)

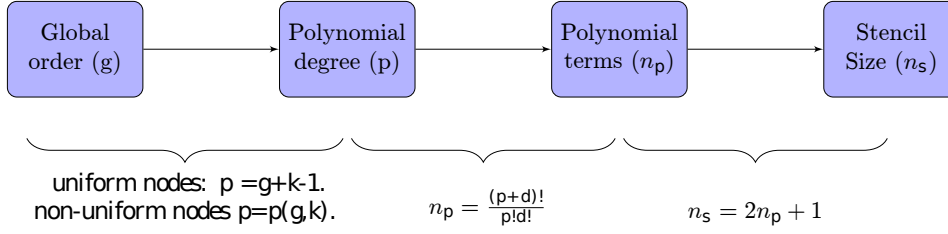


Figure 2.: The process of achieving a global order of convergence in an RBF-FD formulation. That is, the order of convergence is asked by the user and the algorithm decides the degree of polynomial to be augmented, which in turn gives the number of polynomial terms required (n_p) and consequently the stencil size (n_s).

is a limitation in the RBF-FD formulation with pure RBFs. The stagnation error, however, has different interpretations with respect to GA and PHS RBF as explained in [8]. In a purely PHS-based RBF-FD, the stagnation error is mainly due to the large boundary errors. However, if one follows above thumb rules explained in this subsection, with proper polynomial augmentation, the RBF-FD formulation remains free from stagnation error.

3. The RBF-FD (PHS+Poly) under non-uniform node distribution

For quasi-uniform node distribution, the convergence of an RBF-FD method can be estimated in a straightforward manner, that is, by plotting the numerical error against the fill-distance h of X . According to numerical tests performed in [2, 8], for a quasi-uniform nodes, the convergence order of a RBF-FD method is $O(h^{p-k+1})$, where p is the polynomial degree⁴ and k is the order of operator being approximated. However, for a highly non-uniform node-distribution, the relationship of fill distance h and N is different from case to case. Therefore, determining the order of the convergence is not as straightforward. In the follows, we will establish a definition of the global convergence with respect to an effective fill distance by formulating an adaptive RBF-FD approach.

Given a set of points $X = \{\mathbf{x}_1, \dots, \mathbf{x}_N\} \subset \mathbb{R}^d$, its fill distance is given by

$$h_{X,\Omega} := h_X = \sup_{\mathbf{x} \in \Omega} \min_{\mathbf{x}_j \in X} \|\mathbf{x} - \mathbf{x}_j\|_{\ell_2(\mathbb{R}^d)}, \quad (7)$$

the separation distance is

$$q_X := \frac{1}{2} \min_{i \neq j} \|\mathbf{x}_i - \mathbf{x}_j\|_{\ell_2(\mathbb{R}^d)},$$

and $\rho_X = h_X/q_X \geq 1$ is the mesh ratio of X . Quasi-uniform means that, as X refines, ρ_X is bounded for all N . A usual estimation is: $N \sim q_X^{-d}$ for quasi-uniform sets; notation \sim means proportional with some constant.

Adaptive node distributors we proposed end up with (a sequence of) quasi-uniform sets of data points. These sets are expected to have large mesh ratio ρ , which, to users' eyes, are nonuniform and being denser in some problematic spatial region. By the definition of the fill distance, there must be at least one stencil (S_i) in Ω in the coarse

⁴In our context, this degree refers to the fact that all polynomial basis with degree up to p are augmented

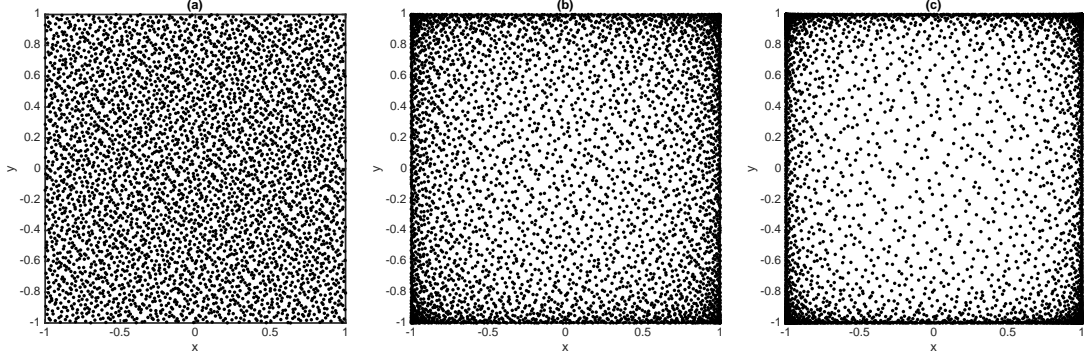


Figure 3.: Node distribution under different mesh ratio with $N = 4096$ (a) quasi-uniform, (b) moderately non-uniform (mesh ratio $\rho_X \sim 10^2$), and (c) highly non-uniform (mesh ratio $\rho_X \sim 10^5$) points in unit square $[-1, 1]^2$.

region with local fill distance being exactly $h_{X,\Omega_i} = h_{X,\Omega}$. If we employ a p^{th} -order RBF-FD approximation scheme, the resulting local error will refine as

$$\varepsilon \sim h_X^p = (\rho_X q_X)^p \sim \rho_X^p N^{-p/d}.$$

For uniform node (with $\rho_X = 1$), the last factor $N^{-p/d}$ ($\sim h_e$) is exactly what we expect from a p -order scheme. In cases when $\rho_X \gg 1$, the p^{th} -asymptotic convergence rate remains p but come with a huge constant ρ_X^p . Figure 3 show the node distribution of $N = 4096$ under mesh ratio $\rho_X = 1, 10^2, 10^5$ respectively.

When approximate an differential operator of order k , we propose a algorithm to obtain g^{th} convergence rate with non-constant augment polynomial order p_i for each node by satisfying

$$h_{X,\Omega_i}^{p_i-k+1} = h_{e,\Omega}^g, \quad (8)$$

where g is the user-defined global convergence rate, $h_{e,\Omega}$ is the effective fill distance, and h_{X,Ω_i} is the local fill distance centered at x_i . The effective fill distance $h_{e,\Omega}$ is computed by number of nodes per unit volume as

$$h_{e,\Omega} = \left(\frac{\text{Vol}(\Omega)}{N} \right)^{1/d},$$

where N is total number of nodes, and d is the dimension of the problem considered. Our next task is to determine the degree of augmented polynomials $p_i = p_i(h_{X,\Omega_i}, h_{e,\Omega}, g)$ for each Ω_i based on the local fill distance h_{X,Ω_i} , effective fill distance $h_{e,\Omega}$, expected global convergence order g , and the operator order k .

Adaptive methods are quite popular in the context of finite element methods (FEM), which have given many version of the algorithms such as h -FEM, p -FEM, or hp -FEM. In order to meet a certain order of accuracy throughout the domain, the idea behind adaptivity is to vary parameters affecting the accuracy of the algorithm locally.

In the follows, we propose a strategy for choosing the locally degree of polynomial p_i to be augmented at a local scale while approximating a k^{th} order differential operator. Given the global fill distance $h_{e,\Omega}$, local fill distance h_{X,Ω_i} , and order of differential operator k , from the (8), the formulation of local polynomials' order to get the g^{th}

Algorithm 1: PSEUDO-CODE FOR COMPUTING AND USING N -ADAPTIVE RBF-FD WEIGHTS

```
1: procedure INPUT( $g \in \mathbb{Z}^+, \mathbf{x} \in \mathbb{R}^d$ )                                 $\triangleright$  Input expected order and nodes
2:   Compute total number of nodes  $N$ 
3:   Compute  $h_{e,\Omega} = \sqrt{\frac{Vol(\Omega)}{N}}$ 
4:   Fix a maximum stencil size  $n_m$ 
5:   Find  $n_m$  – nearest neighbors for each  $\mathbf{x}_i$                                  $\triangleright$  We have used knn-search
6:   Index stencil points as a vector  $\mathbf{x}_s = (x_s, y_s), \mathbf{x}_s \in \mathbb{R}^{d \times n_m}$ 
7:   for (LOOP OVER ALL THE INTERIOR NODES) do
8:      $[w] = \text{Weight2D}[(x, y), g, (x_s, y_s), h_e]$                                  $\triangleright$  Computing Weights for one interior node
9:     Find  $h_{X,\Omega_i}$                                  $\triangleright$  Find local fill-distance
10:     $p_i = g \frac{\log_{10} h_{e,\Omega}}{\log_{10} h_{X,\Omega_i}} + k - 1$                                  $\triangleright$  Polynomial degree required to maintain order  $g$ 
11:     $n_p = C(p + d, d) = \frac{(p+d)!}{p!d!}$                                  $\triangleright$  Number of polynomial basis
12:     $n_s = 2n_p + 1$                                  $\triangleright$  Stencil size just enough to support the polynomial  $p$ 
13:     $r = \sqrt{(x^2 + y^2)}$ 
14:     $A0 = r^m$                                  $\triangleright$  The RBF interpolant
15:     $RHS0 = [rhs_L]$                                  $\triangleright$  This is the RHS column in equation (1)
16:     $A = A0 + Poly(p)$                                  $\triangleright$  The RBF interpolant after augmenting polynomial of degree  $p$ 
17:     $RHS = RHS0 + Poly(p)$                                  $\triangleright$  Adding corresponding polynomial of degree  $p$ 
18:     $w_L = A/RHS$                                  $\triangleright$  Solve the linear system for weights
19:     $w_L = w(1 : n_s)$                                  $\triangleright$  Ignore the weights corresponding to polynomial augmentation
20:  end
21:  for (LOOP OVER ALL THE INTERIOR NODES) do
22:     $L(f) = w_L f$ 
23:  end
24: end
```

convergence rate is as follows:

$$p_i = g \frac{\log_{10} h_{e,\Omega}}{\log_{10} h_{X,\Omega_i}} + k - 1. \quad (9)$$

For quasi-random node-layout ($h_{X,\Omega_i} \approx h_{e,\Omega}$), Equation (9) simplifies to

$$p = g + k - 1 \quad \text{or} \quad g = p - k + 1, \quad (10)$$

that is, the order of an RBF-FD algorithm will be $O(h^{p-k+1})$, which is consistent with the existing literature [2, 8].

For the user-defined convergence rate g , after computing the required number of polynomials p_i by Equation (9) for each local stencil, we can further determine the stencil size $n_s = 2n_p + 1$ as suggested in [2, 8] to ensure the solvability and the stability of our algorithm. Since ‘more than required’ stencil size does not improve the accuracy, in a region with high-node density, from (9), reducing value of p_i allows us to pick a smaller stencil without significantly affecting the accuracy or stability of the RBF-FD discretization. Figure 2 illustrates the adaptive process in our RBFFD scheme. Since the computational cost of the RBF-FD depends on the stencil-size, a smaller local stencil size in the dense part of the domain will correspond to a speed-up in the algorithm. Algorithm 1 is the pseudo-code for computing N -adaptive RBF-FD weights and summarizes the proposed adaptive RBFFD scheme.

4. Numerical experiments

4.1. Example 1: Performance of the adaptive RBF-FD method

In this test, we investigate the adaptive RBF-FD for solving an elliptic partial differential equation. The test problem set up as:

$$\begin{aligned} -\nabla^2 u(x, y) &= f(x, y), & (x, y) \in \Omega, \\ u(x, y) &= \sin(x^2 + y), & (x, y) \in \Gamma_2 := \partial\Omega \setminus \Gamma_1, \\ \frac{\partial u(x, y)}{\partial \mathbf{n}} &= \cos(x^2 + y), & (x, y) \in \Gamma_1, \end{aligned}$$

with domain $\Omega = [-1, 1]^2$ and the boundary $\Gamma_1 : \{(x, y) | -1 \leq x \leq 1, y = 1\}$. The analytical solution and the source term are given, respectively, as

$$u(x, y) = \sin(x^2 + y), \quad f(x, y) = -2 \cos(x^2 + y) - (4x^2 + 1) \sin(x^2 + y).$$

The aim of this numerical test is to demonstrate that an adaptive node-distribution can provide a more accurate solution compared with the solution under the same number of uniform nodes. In such cases, the proposed RBF-FD will be an efficient scheme at a relatively lower cost.

Figure 4 shows interior nodes of $N = 2500$ in Ω with quasi-uniform (left) and non-uniform (right) point-distribution. Non-uniform distributed nodes are obtained by using the transformation $z = (\sin \frac{\pi}{2}(z))$ in each coordination. By setting the global convergence rate $g = 5$ and fixing node number $N = 2500$, the sparsity pattern and eigenvalues of the globally assembled A-matrix through RBF-FD discretization are shown by uniform node distribution in Figure 5 (a-b) and non-uniform distribution in Figure 5 (c-d). It should be noted, for uniform node distribution, the adaptive method is equivalent to the standard RBF-FD. From Figure 5 (a,c), it can be seen that the bandwidth of A-matrix generated from adaptive method is in the range of $[9, 15]$, and the bandwidth by standard RBF-FD is fixed as 12. Except the region near the boundary with denser nodes, the bandwidth by adaptive RBF-FD is narrower than the results by standard RBF-FD. What's more, the number of nonzero elements in the A-matrix by adaptive RBF-FD method becomes $n_Z = 1.12 \times 10^5$, which is around 18% smaller compared with standard RBF-FD method. From Figure 5 (b,d), the real parts of the eigenvalues computed from A-matrix are all positive which shows that the stable numerical approximations can be solved by both standard and proposed adaptive methods.

To verify the convergence behavior of proposed method, we compute the ℓ^2 error of the results by:

$$\ell^2 \text{ error} = \frac{\sqrt{\sum_{i=1}^N (u(x_i) - \hat{u}(x_i))^2}}{N}.$$

Figure 6 shows the comparison result between RBF-FD with uniform nodes and the adaptive RBF-FD with non-uniform nodes under $g = 7$. It can be seen that the adaptive RBF-FD gives higher accuracy while maintaining the desired convergence rate. At the same time, it leads to a more sparse system matrix. For example, with $N = 2500$, the non-zero elements in the system matrix and the corresponding error for

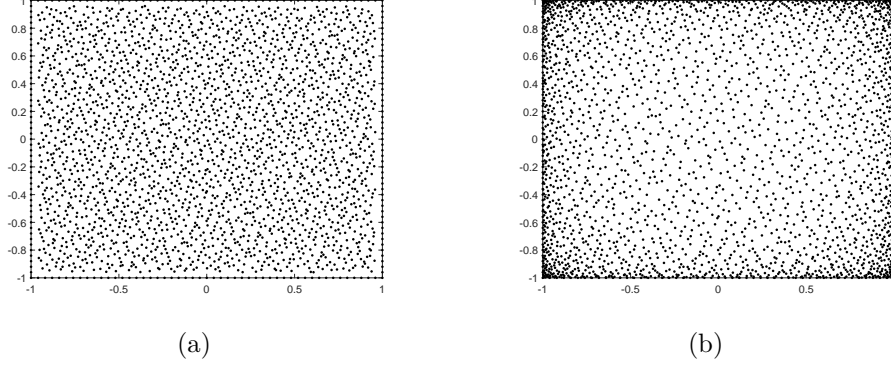


Figure 4.: Example 1: (a) quasi-uniform, and (b) non-uniform distributed nodes in $\Omega = [-1, 1]^2$ with $N = 2500$.

Table 2.: Example 1: by setting convergence rate $g = 7$, the polynomial degree (p_i) chosen by the adaptive algorithm for (a) uniform node distribution and (b) non-uniform node-distribution with $N = 6241$

Polynomial degree (p_i)	5	6	7	8
RBF-FD	0	0	0	6241
Adaptive RBF-FD	110	1727	2694	1710

the adaptive RBF-FD are $n_z = 1.08 \times 10^5$, $L^2 \text{ Error} = 7.79 \times 10^{-9}$, while the results for the standard RBF-FD are $n_z = 1.37 \times 10^5$, $L^2 \text{ Error} = 1.04 \times 10^{-6}$. Therefore, the accuracy does not influenced compared with standard RBF-FD. By setting $g = 7$, Table 2 shows the frequency of polynomial degree during overall weight computation. For a uniform set and a non-uniform set with $N = 6241$, the polynomial degree remains $p = 8$ for the former, which equals to the global order $g + 1$. However, the polynomial degree is selected from range $p = 5$ to $p = 8$ for non-uniform nodes, depending on the local node-density.

We conclude that the advantage of using the adaptive RBF-FD is twofold: (i) it resolves the physics of the problem with a much better accuracy; and (ii) the number of non-zero elements in the A-matrix of the resulting system are relatively smaller because it uses smaller stencils in the sub-domains having higher node-density. The advantage (ii) would become more important for solving large-scale problems using sparse linear solvers.

4.2. Example 2: Benchmark test

In this part, we consider a benchmark test problem designed to test adaptive FEM algorithms by US National Institute for Standards and Technology (NIST) [19]. The test problem is a Poisson equation in $[0, 1]^2$, which has an exponential peak in the domain and non-constant Dirichlet boundary conditions matching the exact solution given by

$$-\Delta u(x, y) - f(x, y) = 0 \quad \text{in} \quad \Omega = [0, 1]^2,$$

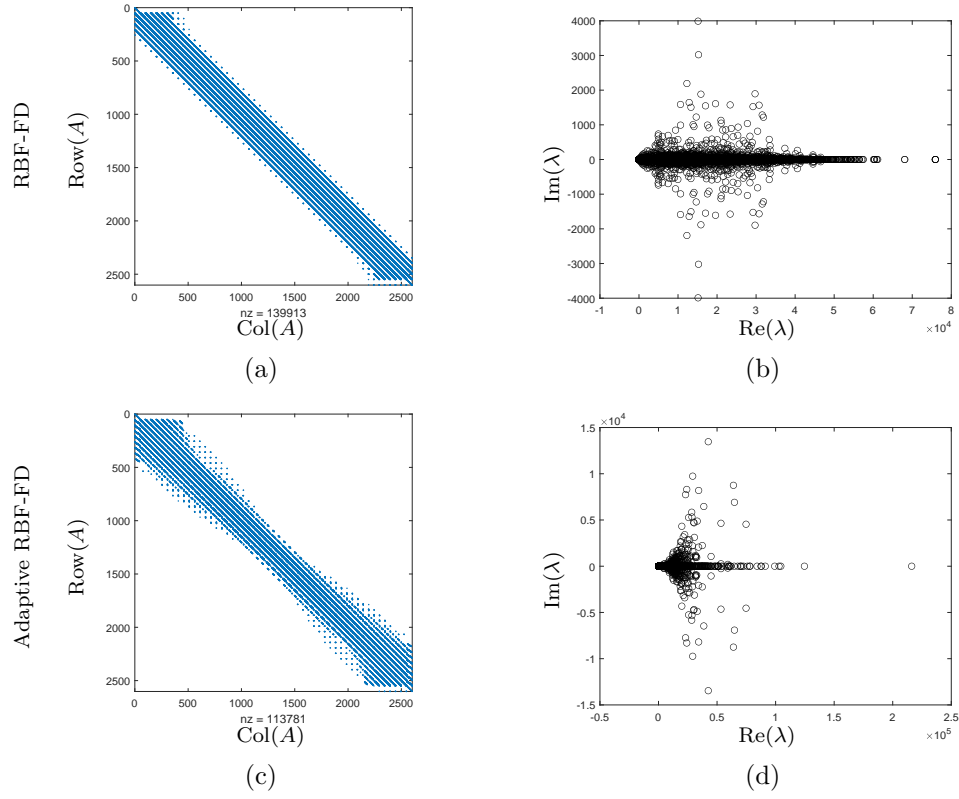


Figure 5.: Example 1: by adaptive RBF-FD for uniform nodes and non-uniform node distribution, (a,c): Sparsity pattern and (b,d): eigenvalue spectra of the system matrix, respectively.

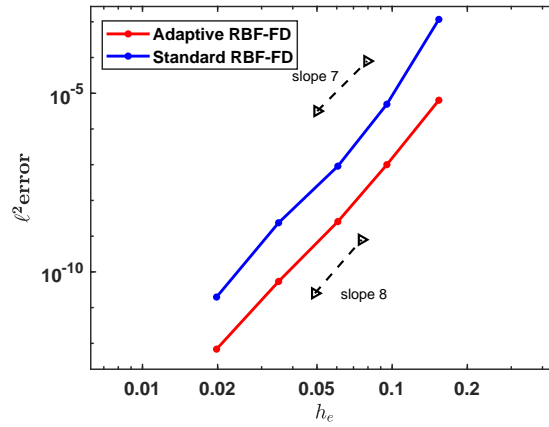


Figure 6.: Example 1: Comparison of the convergence of RBF-FD with uniform nodes and the adaptive RBF-FD with non-uniform nodes

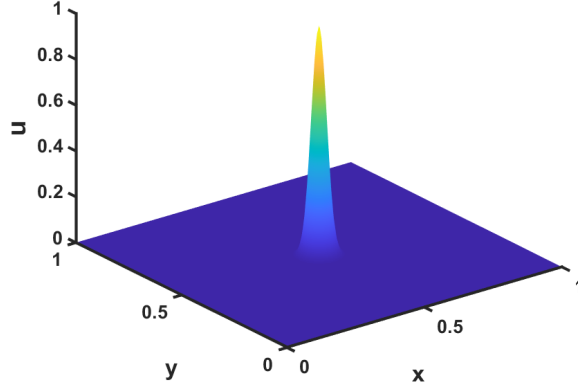


Figure 7.: Example 2: A reference solution with $\alpha = 1000$ and $(x_c, y_c) = (0.5, 0.5)$

and the exact solution

$$u(x, y) = e^{-\alpha((x-x_c)^2+(y-y_c)^2)},$$

where (x_c, y_c) is the location of the peak and α determines the strength of the peak. A typical value $\alpha = 1000$ is suggested to test an adaptive algorithm. The right hand side function $f(x, y)$ satisfying the exact solution is given as

$$f(x, y) = -4e^{-\alpha((x-x_c)^2+(y-y_c)^2)} (\alpha^2(x-x_c)^2 + \alpha^2(y-y_c)^2 - \alpha)$$

The reference solution with $\alpha = 1000$ is shown in the Figure 7. For PDE-dependent node generation, we used **NodeLab**. Firstly, we solve the problem with standard RBF-FD approach over quasi-uniform nodes in the domain and a fixed polynomial degree ($p = 6$). Figures 8 (a,b,c) show the uniform node-distribution ($N = 2470$), approximated solution and point-wise absolute error, respectively. It is evident from the error plot that the approximation error is maximum in the peak zone of the sub-domain. Figures 8 (d) shows an adaptive node-distribution with same number $N = 2470$, which is denser in the peak zone. This adaptive node-distribution enhance the accuracy in the approximation. Figures 8 (e,f) show the approximated solution and point-wise absolute error with an expected global order ($g = 5$). It is obviously the accuracy by adaptive RBF-FD is improved in the peak zone compared with standard RBF-FD. By setting convergence rate $g = 5$, Figure 9 shows the results of standard and adaptive RBF-FD method by computing L^∞ error as

$$\ell^\infty \text{ error} = \max_{1 \leq i \leq N} |u(x_i) - \hat{u}(x_i)|.$$

We can see that 5^{th} convergence rate is obtained by both method. Furthermore, the proposed adaptive method can have higher accuracy.

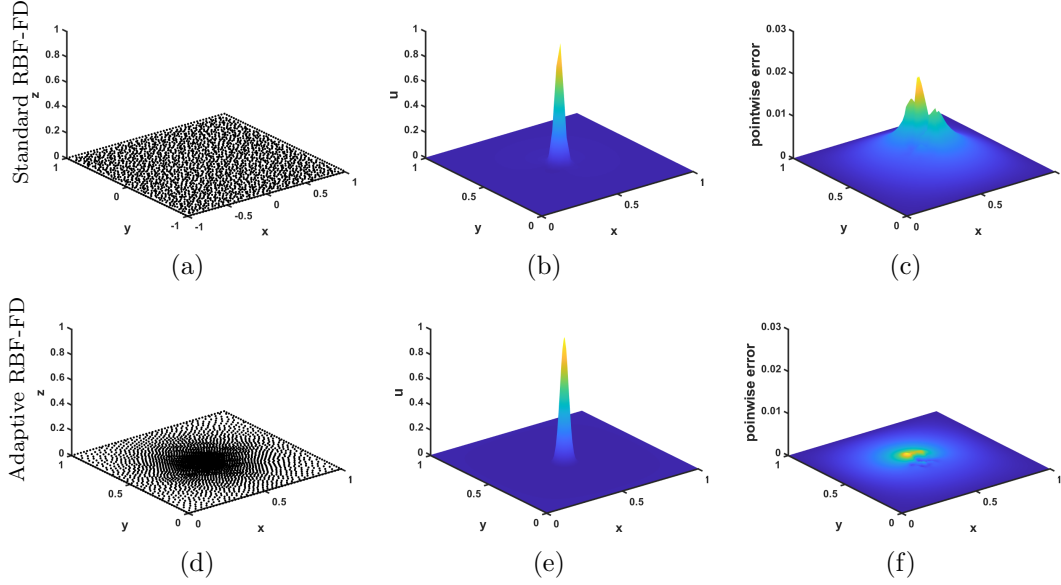


Figure 8.: Example 2: By $N = 2470$, the first row shows the (a) node-distribution, (b) approximated solution, and (c) pointwise absolute error in the approximated solution, respectively with standard RBF-FD approach by polynomial degree $p = 6$. The second row shows the same results for adaptive RBF-FD with variable polynomial degree p corresponding to a desired order $g = 5$ in (d)–(f), respectively.

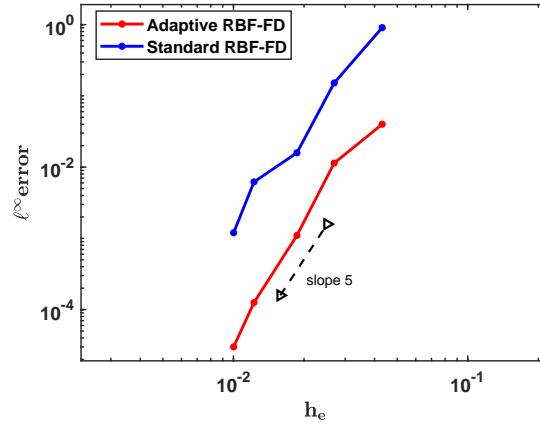


Figure 9.: Example 2: Comparison of convergence of the standard RBF-FD and the Adaptive RBF-FD for a Poisson equation with delta-like exact solution.

4.3. Example 3: Application in solving time-dependent equations

In this part, we consider the following time-dependent equation incorporated initial and boundary conditions as

$$\begin{cases} u_t - \Delta u = f(x, y, t) & \text{for } (x, y, t) \in \Omega \times (0, T], \\ u(x, y, 0) = g_1(x, y) & \text{for } (x, y) \in \Omega, \\ u(x, y, t) = g_2(x, y, t) & \text{for } (x, y, t) \in \partial\Omega \times (0, T]. \end{cases} \quad (11)$$

The domain set as $\Omega = [-1, 1]^2$. The exact solution is given as $u^*(x, y, t) = \exp(t) \cos(\pi x) \cos(\pi y)$. The initial condition and boundary conditions are generated from the exact solution as

$$g_1(x, y) = \cos(\pi x) \cos(\pi y), \quad g_2(x, y, t) = \exp(t) \cos(\pi x) \cos(\pi y).$$

The source term is computed from the exact solution is $f(x, y, t) = (1 + 2\pi^2)u^*(x, y, t)$. For time discretization, after dividing the interval $[0, T]$ by the partition $\{t_n\}_{n=1}^M$ where $t_n = n\tau$ and $\tau = T/M$, we apply the θ -method as

$$\frac{u^n - u^{n-1}}{\tau} = \theta(\Delta u^n + f^n) + (1 - \theta)(\Delta u^{n-1} + f^{n-1}).$$

When $\theta = 1/2$, it is called the Crank-Nicolson method as

$$u^n - \frac{\tau}{2} \Delta u^n = u^{n-1} + \frac{\tau}{2} \Delta u^{n-1} + \frac{\tau}{2} \Delta (f^n + f^{n-1}),$$

and when $\theta = 1$, the backward-Euler scheme is obtained as:

$$u^n - \tau \Delta u^n = u^{n-1} + \tau f^n(x, y, t).$$

The non-uniform discrete points in the domain is generated by the same method as described in Example 1. The user-defined global convergence rate is $g = 5$ and PHS kernel is $\phi(r) = r^{2m-1}$, $m = 3$. Figure 10 illustrate the convergence behavior of the solutions by the $\ell^\infty(\Omega, T)$ error. Figure 10 (a) plots the space convergence results by $\tau = 1E - 7, T = 1E - 6$, discrete points in domain nodes $N = [10, 25, 36, 49, 64]^2$. The local stencil is set as $n_s = 100$. The result shows that the convergence rate $g = 5$ is obtained which is consistent with the required accuracy. Figure 10 (b) illustrates the time convergence results by $T = 1, n_Z = 64^2$. It can be seen that second-order accuracy in time is obtained for the Crank-Nicolson method, and the backward-Euler method is first-order accurate in time. We conclude that the proposed method can be applied to solve time-dependent problems.

4.4. Example 4: Application in elastic wave model

In this part, we apply the adaptive RBF-FD method to the following elastic wave Navier equation:

$$\begin{cases} \mu \Delta u_1 + (\lambda + \mu) \left(\frac{\partial^2 u_1}{\partial x^2} + \frac{\partial^2 u_2}{\partial x \partial y} \right) + \omega^2 \rho u_1 = f_1 \\ \mu \Delta u_2 + (\lambda + \mu) \left(\frac{\partial^2 u_1}{\partial x \partial y} + \frac{\partial^2 u_2}{\partial x^2} \right) + \omega^2 \rho u_2 = f_2 \end{cases}, \quad (12)$$

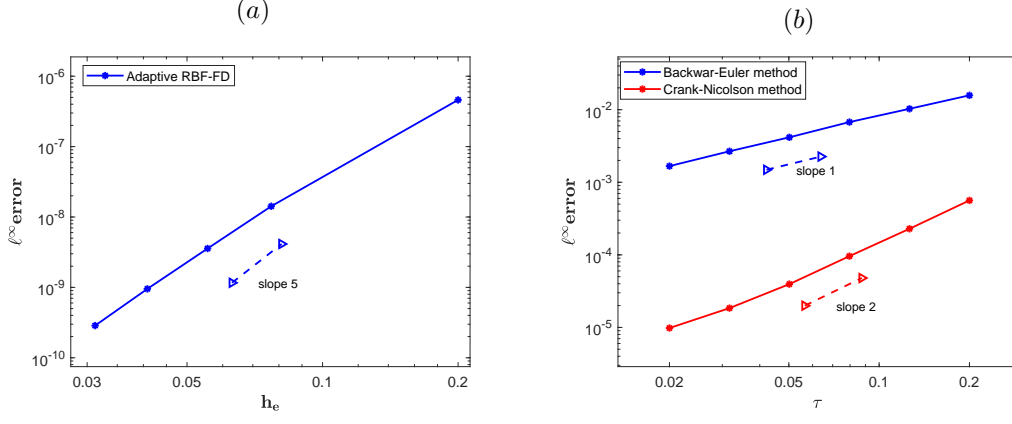


Figure 10.: Example 3: the convergence behavior of adaptive RBFFD by solving the heat equation (11) (a) space convergence by $\tau = 1E-7$, $T = 1E-6$, $n_Z = [10, 25, 36, 49, 64]^2$; (b) time convergence by $\tau \in [0.02, 0.2]$, $T = 1$, $n_Z = 64^2$

with ω being the angular frequency and λ , μ being Lamé constants. Under the assumption of homogeneous medium, we prescribe the density $\rho \equiv 1$ for simplicity in calculation. The time-harmonic displacement vector $\mathbf{u} = (u_1, u_2)^T$ satisfies the lowest-order absorbing boundary condition:

$$\mathbf{T}^{(n)}(\mathbf{u}) - i\eta\mathbf{u} = \mathbf{g} \quad \text{on } \gamma = \partial\Omega,$$

where the traction operator $\mathbf{T}^{(n)}$ is

$$\mathbf{T}^{(n)}(\mathbf{u}) = 2\mu \frac{\partial \mathbf{u}}{\partial \mathbf{n}} + \lambda \mathbf{n} \nabla \cdot \mathbf{u} + \mu \mathbf{n} \times (\nabla \times \mathbf{u}),$$

with \mathbf{n} being the unit normal vector and a real-valued matrix function η is defined by

$$\eta = \omega \rho (C_P \mathbf{n} \otimes \mathbf{n} + C_S \mathbf{s} \otimes \mathbf{s}), \quad C_P = \sqrt{\frac{\lambda + 2\mu}{\rho}}, \quad C_S = \sqrt{\frac{\mu}{\rho}}$$

with \mathbf{s} being a unit tangential vector. Similar problems are considered in [30]. We study the Navier equation in the square domain $\Omega = [0, 1]^2$, non-uniform distribution nodes are obtained by using the transformation $z = \frac{1}{2} \sin(\pi z) + \frac{1}{2}$. The components of the exact displacement field $\mathbf{u} = (u_1, u_2)^T$ is given as follows

$$\begin{cases} u_1 = \alpha_S \left\{ e^{-\alpha_S y} - \frac{2\kappa_R^2}{\kappa_R^2 + \alpha_S^2} e^{-\alpha_P y} \right\} e^{i\kappa_R x} \\ u_2 = i\kappa_R \left\{ e^{-\alpha_S y} - \frac{2\alpha_P \alpha_S}{\kappa_R^2 + \alpha_S^2} e^{-\alpha_P y} \right\} e^{i\kappa_R x}, \end{cases} \quad (13)$$

where $\alpha_P = \sqrt{\kappa_R^2 - \kappa_P^2}$, $\alpha_S = \sqrt{\kappa_R^2 - \kappa_S^2}$. We take the Lamé constants $\lambda = 2$, $\mu = 1$, angular frequency $\omega = 2\pi$, which decide the value of $\kappa_R = 2.14\pi$; $\kappa_P = \pi$; $\kappa_S = 2\pi$. We measure the accuracy of the numerical solution through the following relative numerical error:

$$E_\eta = \frac{|\mathbf{u}^e - \mathbf{u}^n|_1}{|\mathbf{u}^e|_1} = \sqrt{\frac{\int_\Omega (\overline{\mathbf{u}}^e - \overline{\mathbf{u}}^n)^T (\mathbf{u}^e - \mathbf{u}^n) d\Omega}{\int_\Omega (\overline{\mathbf{u}}^e)^T (\mathbf{u}^e) d\Omega}},$$

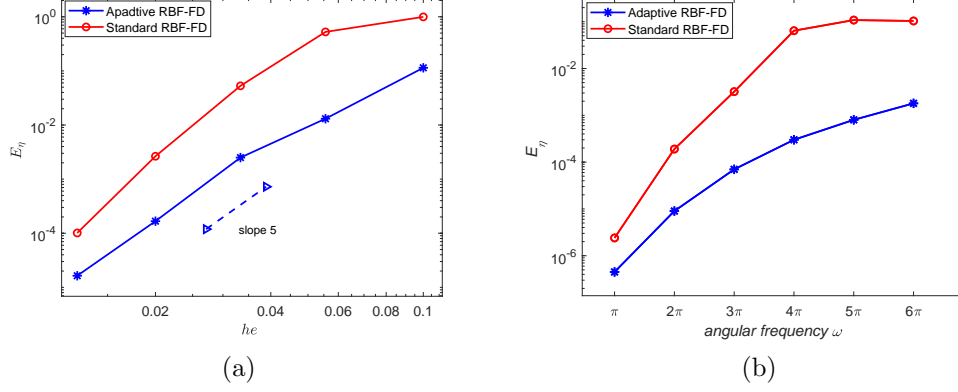


Figure 11.: Example 4: (a) Comparison of convergence of the standard RBF-FD and the Adaptive RBF-FD for Navier equation. (b) The relative errors using different methods against the angular frequencies for the Navier equation.

We set the global convergence order as $g = 5$, and the maximum stencil size set as $n_s = 100$. With the proposed adaptive method, Figure 11 (a) shows the relative error with respect to the global fill distance. We can see that more precise result with required convergence rate is obtained compared with standard RBF-FD method. The angular frequency ω is an important parameter of the elastic wave equation, which determines the oscillatory behavior of the solution. The angular frequencies become larger, the oscillations become more frequently. The profile of errors E_η at different ω are shown in Figure 11 (b). The results demonstrate that the solutions progressively deteriorate as angular frequencies increase. However, the adaptive RBF-FD is less sensitive to angular frequency compared with standard RBF-FD. By $N = 3600$, Figure 12 plots the numerical and analytical solutions of u_1 , u_2 at the circle $r = 0.5$ versus the polar angle, the real part and imaginary part of u_1 , u_2 are plotted separately. It can be clearly observed from these figures that the numerical solutions obtained by adaptive RBF-FD recover the analytic solutions well.

For the linear system with $g = 5$ by uniform and adaptive RBF-FD, the number of nonzero elements are $n_1 = 8.2 \times 10^5$ and $n_2 = 6.5 \times 10^5$, i.e., a reduction of $n_1 - n_2 = 1.7 \times 10^5$ nonzero elements. We can conclude that the adaptive RBF-FD can save calculation cost compared with the uniform case, and this advantage will be more obvious as the order of convergence increases. When convergence order $g = 7$, adaptive RBF-FD reduces the total nonzero elements in the A-matrix by 2.3×10^5 . The Realistic elastic wave models are more complicated requiring non-uniform node-distribution. Therefore, the present adaptive RBF-FD method could be an efficient algorithm.

5. Conclusions

In this paper, we propose an adaptive version of RBF-FD (PHS+poly) approach, which is better suited for the problems requiring high-order approximation over highly non-uniform node-distributions. When the node-distribution is uniform, the adaptive RBF-FD method simplifies to the standard RBF-FD approach. We define the adaptive RBF-FD over non-uniform node-distributions with a user defined global convergence order. Through the numerical tests performed in this paper, for a fixed number of

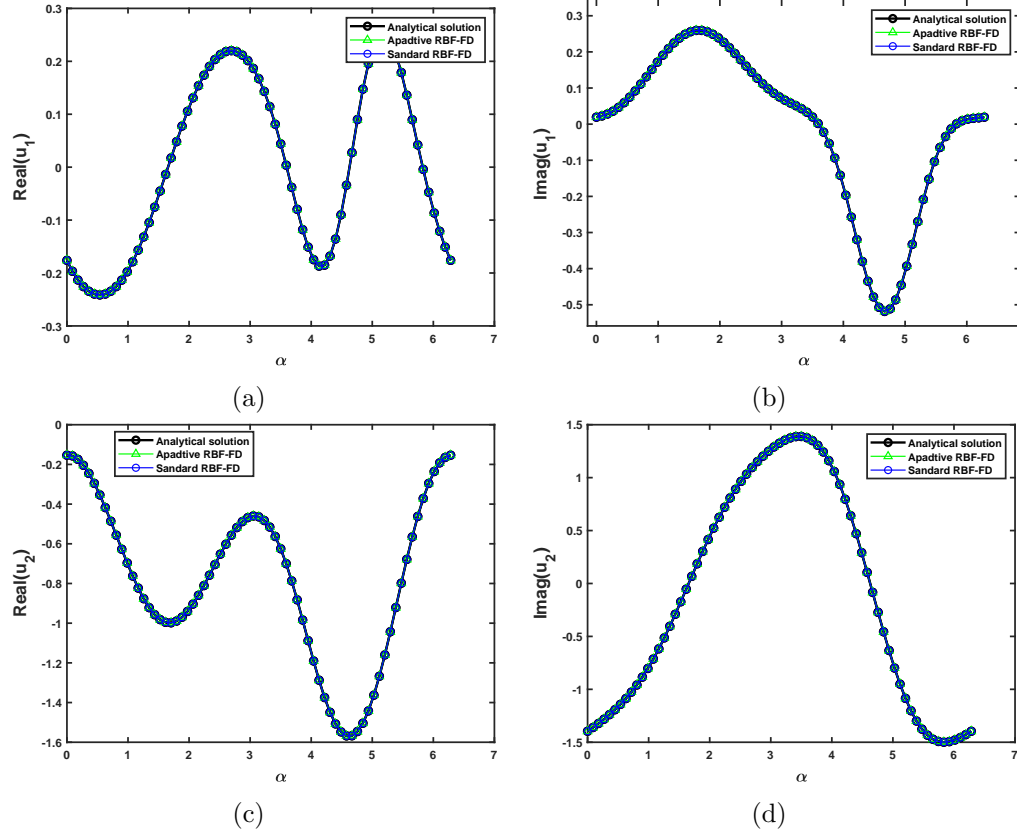


Figure 12.: Example4: results by adaptive RBF-FD for the Navier equation with $\omega = 2\pi$ and $N = 3600$.

nodes in the domain, it has been shown that the adaptive RBF-FD with non-uniform nodes distributions provides a better numerical approximation than the standard RBF-FD with quasi-uniform nodes. At the same time, the adaptive RBF-FD significantly reduces the number of non-zero elements in the resultant linear system, suggesting a cheaper computational cost. The adaptive RBF-FD approximately maintains a user defined global convergence order even for highly non-uniform nodes. The paper also apply the adaptive RBFFD to the time-dependent problem and elastic wave problems in geophysics to show its further applications.

Acknowledgements

This work was funded by the Hong Kong Research Grant Council GRF Grants (12303818,12301419,12301520,12301021), a National Youth Science Foundation of China (12201449).

References

- [1] V. BAYONA, N. FLYER, AND B. FORNBERG, *On the role of polynomials in RBF-FD approximations: III. behavior near domain boundaries*, Journal of Computational Physics, (2019).
- [2] V. BAYONA, N. FLYER, B. FORNBERG, AND G. A. BARNETT, *On the role of polynomials in RBF-FD approximations: II. numerical solution of elliptic PDEs*, Journal of Computational Physics, 332 (2017), pp. 257–273.
- [3] V. BAYONA, M. MOSCOSO, M. CARRETERO, AND M. KINDELAN, *RBF-FD formulas and convergence properties*, Journal of Computational Physics, 229 (2010), pp. 8281–8295.
- [4] G. CHANDHINI AND Y. SANYASIRAJU, *Local RBF-FD solutions for steady convection–diffusion problems*, International Journal for Numerical Methods in Engineering, 72 (2007), pp. 352–378.
- [5] B. ŠARLER, *A radial basis function collocation approach in computational fluid dynamics*, Cmes-computer Modeling in Engineering & Sciences, 7 (2005), pp. 185–194.
- [6] B. ŠARLER AND R. VERTINK, *Meshfree explicit local radial basis function collocation method for diffusion problems*, Computers & Mathematics with Applications, 51 (2006), pp. 1269–1282.
- [7] P. P. CHINCHAPATNAM, K. DJIDJELI, P. NAIR, AND M. TAN, *A compact RBF-FD based meshless method for the incompressible Navier–Stokes equations*, Proceedings of the Institution of Mechanical Engineers, Part M: Journal of Engineering for the Maritime Environment, 223 (2009), pp. 275–290.
- [8] N. FLYER, B. FORNBERG, V. BAYONA, AND G. A. BARNETT, *On the role of polynomials in RBF-FD approximations: I. interpolation and accuracy*, Journal of Computational Physics, 321 (2016), pp. 21–38.
- [9] N. FLYER, E. LEHTO, S. BLAISE, G. B. WRIGHT, AND A. ST-CYR, *A guide to RBF-generated finite differences for nonlinear transport: Shallow water simulations on a sphere*, Journal of Computational Physics, 231 (2012), pp. 4078–4095.
- [10] B. FORNBERG AND N. FLYER, *Solving PDEs with radial basis functions*, Acta Numerica, 24 (2015), pp. 215–258.
- [11] B. FORNBERG AND E. LEHTO, *Stabilization of RBF-generated finite difference methods for convective PDEs*, Journal of Computational Physics, 230 (2011), pp. 2270–2285.
- [12] M. KINDELAN, D. ÁLVAREZ, AND P. GONZALEZ-RODRIGUEZ, *Frequency optimized RBF-FD for wave equations*, Journal of Computational Physics, (2018).
- [13] B. MARTIN, A. ELSHERBENI, G. E. FASSHAUER, AND M. HADI, *Improved FDTD method around dielectric and PEC interfaces using RBF-FD techniques*, in Applied Computa-

- tional Electromagnetics Society Symposium (ACES), 2018 International, IEEE, 2018, pp. 1–2.
- [14] B. MARTIN AND B. FORNBERG, *Using radial basis function-generated finite differences (RBF-FD) to solve heat transfer equilibrium problems in domains with interfaces*, Engineering Analysis with Boundary Elements, 79 (2017), pp. 38–48.
 - [15] B. MARTIN, B. FORNBERG, AND A. ST-CYR, *Seismic modeling with radial-basis-function-generated finite differences*, Geophysics, 80 (2015), pp. T137–T146.
 - [16] P. MISHRA, S. NATH, G. FASSHAUER, AND M. SEN, *Frequency-domain meshless solver for acoustic wave equation using a stable radial basis-finite difference (RBF-FD) algorithm with hybrid kernels*, in SEG Technical Program Expanded Abstracts 2017, Society of Exploration Geophysicists, 2017, pp. 4022–4027.
 - [17] P. K. MISHRA, *NodeLab— a matlab package for meshfree node-generation and adaptive refinement*, (2019). <https://github.com/pankajkmishra/NodeLab>.
 - [18] P. K. MISHRA, G. E. FASSHAUER, M. K. SEN, AND L. LING, *A stabilized radial basis-finite difference (RBF-FD) method with hybrid kernels*, Computers & Mathematics with Applications, (2018).
 - [19] W. F. MITCHELL, *A collection of 2D elliptic problems for testing adaptive grid refinement algorithms*, Applied mathematics and computation, 220 (2013), pp. 350–364.
 - [20] A. PETRAS, L. LING, AND S. J. RUUTH, *An RBF-FD closest point method for solving PDEs on surfaces*, Journal of Computational Physics, 370 (2018), pp. 43–57.
 - [21] L. SANTOS, N. MANZANARES-FILHO, G. MENON, AND E. ABREU, *Comparing RBF-FD approximations based on stabilized Gaussians and on polyharmonic splines with polynomials*, International Journal for Numerical Methods in Engineering, (2017).
 - [22] R. SCHABACK, *A computational tool for comparing all linear PDE solvers*, Advances in Computational Mathematics, 41 (2014), pp. 333–355.
 - [23] ———, *Error Analysis of Nodal Meshless Methods*, Springer International Publishing, 04 2017, pp. 117–143.
 - [24] V. SHANKAR, *The overlapped radial basis function-finite difference (RBF-FD) method: A generalization of RBF-FD*, Journal of Computational Physics, 342 (2017), pp. 211–228.
 - [25] V. SHANKAR, G. B. WRIGHT, R. M. KIRBY, AND A. L. FOGELSON, *A radial basis function (RBF)-finite difference (FD) method for diffusion and reaction–diffusion equations on surfaces*, Journal of scientific computing, 63 (2015), pp. 745–768.
 - [26] J. SLAK AND G. KOSEC, *Refined RBF-FD solution of linear elasticity problem*, in 2018 3rd International Conference on Smart and Sustainable Technologies (SpliTech), IEEE, 2018, pp. 1–6.
 - [27] A. TOLSTYKH AND D. SHIROBOKOV, *On using radial basis functions in a “finite difference mode” with applications to elasticity problems*, Computational Mechanics, 33 (2003), pp. 68–79.
 - [28] G. B. WRIGHT, *Radial basis function interpolation: numerical and analytical developments*, PhD thesis, University of Colorado at Boulder, 2003.
 - [29] G. B. WRIGHT AND B. FORNBERG, *Scattered node compact finite difference-type formulas generated from radial basis functions*, Journal of Computational Physics, 212 (2006), pp. 99–123.
 - [30] L. YUAN AND Y. LIU, *A trefftz-discontinuous galerkin method for time-harmonic elastic wave problems*, Computational and Applied Mathematics, 38 (2019), pp. 1–29.
 - [31] S. ZHANG, *Meshless symplectic and multi-symplectic local rbf collocation methods for hamiltonian pdes*, Journal of Scientific Computing, 88 (2021), p. 90.